

<https://doi.org/10.1038/s43247-024-01417-4>

# Density and strength variations in the mantle lithosphere affect the distribution of intraplate earthquakes

Check for updates

Judith Bott<sup>1</sup> ✉, Magdalena Scheck-Wenderoth<sup>1,2</sup>, Ajay Kumar<sup>1</sup>, Mauro Cacace<sup>1</sup>, Sebastian Noe<sup>3</sup> & Jan Inge Faleide<sup>4</sup>

The distribution of earthquakes in stable intracontinental tectonic settings is typically far more diffuse than along plate boundaries and the causative mechanisms underlying some recognizable clustering are not understood. Here we show that seismicity in intraplate western and central Europe is largely limited to regions that exhibit a low-density layer in the uppermost lithospheric mantle and preferentially clustered above lateral gradients in upper mantle effective viscosity. The basis for these new insights into the thermal and density configuration of the upper mantle is provided by a shear-wave tomographic model. We propose that the spatial correlations between mantle low-density bodies and crustal seismicity reflect the importance of buoyancy forces within the mantle lithosphere. In addition, under the interaction of forces due to mantle gravitational instabilities, plate tectonics and postglacial rebound, the variably hot and strong mantle lithosphere responds by localized deformation which imposes differential loading on the overlying crust.

Unraveling the causative dynamics of continental intraplate seismicity is difficult since these settings overall show low levels of deformation rates, longer return periods for large earthquakes, and more spatially distributed hypocenters than observed along plate boundaries<sup>1</sup>. Stable western and central Europe from the northern Alpine foreland across northwestern France to the British Isles is such an intracontinental domain, where low geodetic strain rates<sup>2</sup> are hard to reconcile with the heterogeneously distributed seismic activity<sup>3</sup> (Fig. 1). Nevertheless, the unknown mechanisms behind this enigmatic seismicity pose a threat to the densely populated region where seismic hazard is not in the public perception because of the long recurrence times of seismic events. As a consequence of the plate tectonic framework involving the North Atlantic opening and the convergence between the African and the European plates, focal mechanisms indicate a dominant north-west directed maximum horizontal stress<sup>4</sup> ( $S_{Hmax}$ ). In addition to plate boundary forces, deformation in the area is potentially also influenced by stresses related to (post)glacial isostatic adjustments (GIA) in the proximity of the once glaciated and currently uplifting regions of Fennoscandia, the northern British Isles, and the Alpine belt<sup>5</sup>. How these different factors interact over time and space and thereby

control the lateral distribution of seismic activity today, however, is still not comprehensively explained.

In response to a polyphase tectonic history of the region, the crust exhibits various sets of differently aged, internal tectonic boundaries and major faults (Fig. 1). Some of these discontinuities have been suggested to have driven the localization of recent deformation, in particular, the European Cenozoic Rift System<sup>6</sup> (ECRIS), Mesozoic inversion structures situated between the ECRIS and the Trans-European Suture Zone<sup>7</sup> and Paleozoic crustal sutures of northwestern France<sup>8</sup> and the British Isles<sup>9</sup>. The majority of earthquakes in the region, however, cannot unequivocally be mapped to specific crustal-scale discontinuities; nor are they restricted to domains of weaker crust as assessed by geophysical data-based thermal and rheological modeling<sup>10</sup>.

Based on GNSS-derived velocity field models, it was estimated that vertical strain rates in the study area result to a great extent from buoyancy-driven forces sourced in the mantle and suggested that the latter would play an important role also in localizing seismicity clusters<sup>2</sup>. Furthermore, variations in the thickness, temperature, and thus strength of the whole lithosphere as inferred from a surface-wave tomography model have been

<sup>1</sup>Helmholtz Centre Potsdam—GFZ German Research Centre for Geosciences. Telegrafenberg, 14473 Potsdam, Germany. <sup>2</sup>RWTH Aachen, Faculty of Geosciences and Materials Engineering. Lochnerstr. 4-20, 52056 Aachen, Germany. <sup>3</sup>ETH Zürich, Department of Earth Sciences. Sonneggstrasse 5, 8092, Zürich, Switzerland. <sup>4</sup>University of Oslo, Department of Geosciences. Sem Sælands vei 2A, Blindern, N-, 0371 Oslo, Norway.

✉ e-mail: [judith.bott@gfz-potsdam.de](mailto:judith.bott@gfz-potsdam.de)

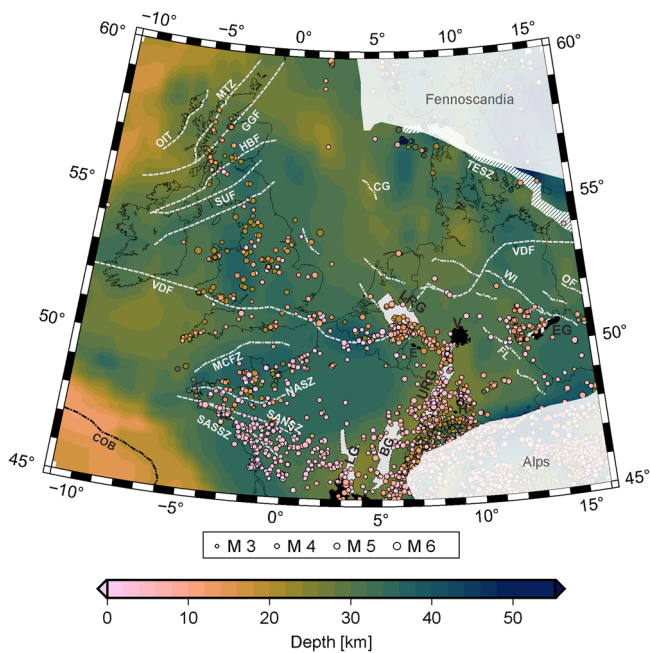


**Fig. 1 | Crustal configuration and tectonic structures of Western and central Europe.** Background color is for the depth of the crust-mantle boundary (Moho; EuCrust07 model<sup>65</sup>). Circles mark the depth and magnitude of seismic events (moment magnitudes  $\geq M3$  of the ESHM20 catalog<sup>3</sup>). Grayed-out regions of the Alps and Fennoscandia are not discussed here because of the larger vertical strain rates related to ongoing glacial isostatic adjustments<sup>2</sup>. Also shown are selected tectonic elements proposed by other studies to be related to present-day seismicity (see main text): Paleozoic structures (dashed), Mesozoic structures (dashed-dotted), Cenozoic grabens (gray-filled) and Cenozoic volcanic fields (black-filled). TESZ Trans-European Suture Zone. Terrane bounding faults of the British Isles<sup>86</sup>: GGF Great Glen Fault, HBF Highland Boundary Fault, MTZ Moine Thrust, OIT Outer Isles Thrust, SUF Southern Uplands Fault; terrane bounding faults of NW France<sup>87</sup>: MCFZ Mid-Channel Fault Zone, N/SASZ North/South Armorican Shear Zone, SASSZ South Armorican Southern Shear Zone, VDF Variscan Deformation Front<sup>88</sup>, inversion structures of the Alpine foreland<sup>89</sup>: CG Central Graben western fault, FL Franconian Line, OF Odra Fault, WI Wittenberg Fault; elements of the European Cenozoic Rift System (ECRIS)<sup>90</sup>: LG Limagne Graben, BG Bresse Graben, URG Upper Rhine Graben, LRG Lower Rhine Graben, MC Massif Central, H Hegau, V Vogelsberg, E Eifel, EG Eger Graben; COB crustal continent-ocean boundary<sup>91</sup>.

proposed to explain the differences in seismic activity between (less active) Ireland and mainland Britain<sup>11</sup>. A causal relationship between clustered seismicity in the crust and seismologically imaged low-velocity zones in the mantle below has also been proposed for other intracontinental settings such as Australia<sup>12</sup> or the New Madrid Seismic Zone in the southeastern United States<sup>13</sup>. What is missing so far, however, for our study area and other stable interiors as well is a quantification of the thermal configuration and related strength and density variations across the whole mantle lithosphere.

In this paper, we quantitatively explore and discuss the potential effects of upper mantle heterogeneities on the lateral distribution of earthquakes across stable western and central Europe. Therefore, we derive variations in temperature from a continent-scale tomographic shear-wave velocity ( $v_s$ ) model, which is the updated Collaborative Seismic Earth Model, CSEM Europe<sup>14</sup>. This allows us to directly estimate the related efficiency of viscous creep in the mantle (effective viscosity) as a proxy for spatial variations in the mantle susceptibility to deformation. Through the conversion approach chosen to use (Methods), we additionally obtain the upper mantle density configuration, which (i) is non-linearly related to temperature as reflected in the differing vertical anomaly patterns and (ii) provides an indicator for a key component potentially contributing to spatial variations in gravitational potential energy and buoyancy forces.

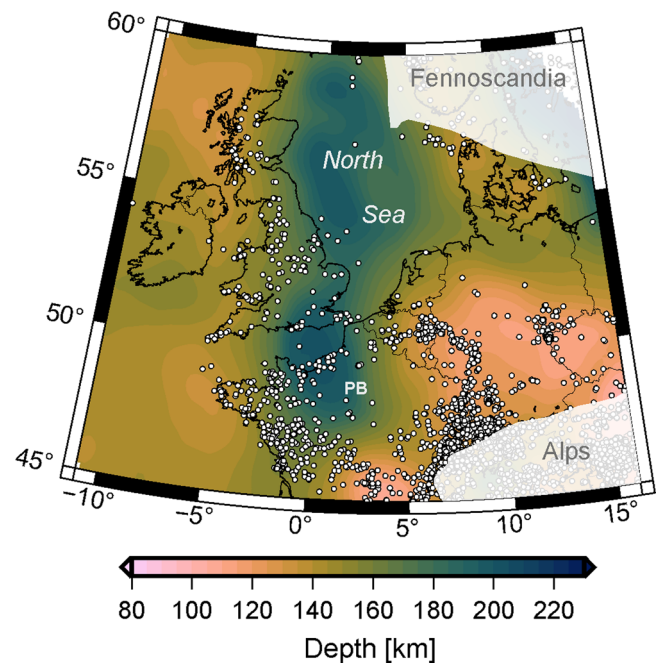


**Fig. 2 | Thermal lithosphere-asthenosphere boundary (LAB).** This interface corresponds to the depth of the 1300 °C-isotherm derived from the thermal configuration as obtained by converting shear-wave velocities of the full-waveform inversion-derived model CSEM Europe<sup>14</sup> to temperatures; white dots are hypocenter locations of the ESHM20 seismic catalog<sup>3</sup>. PB Paris Basin mantle thermal anomaly.

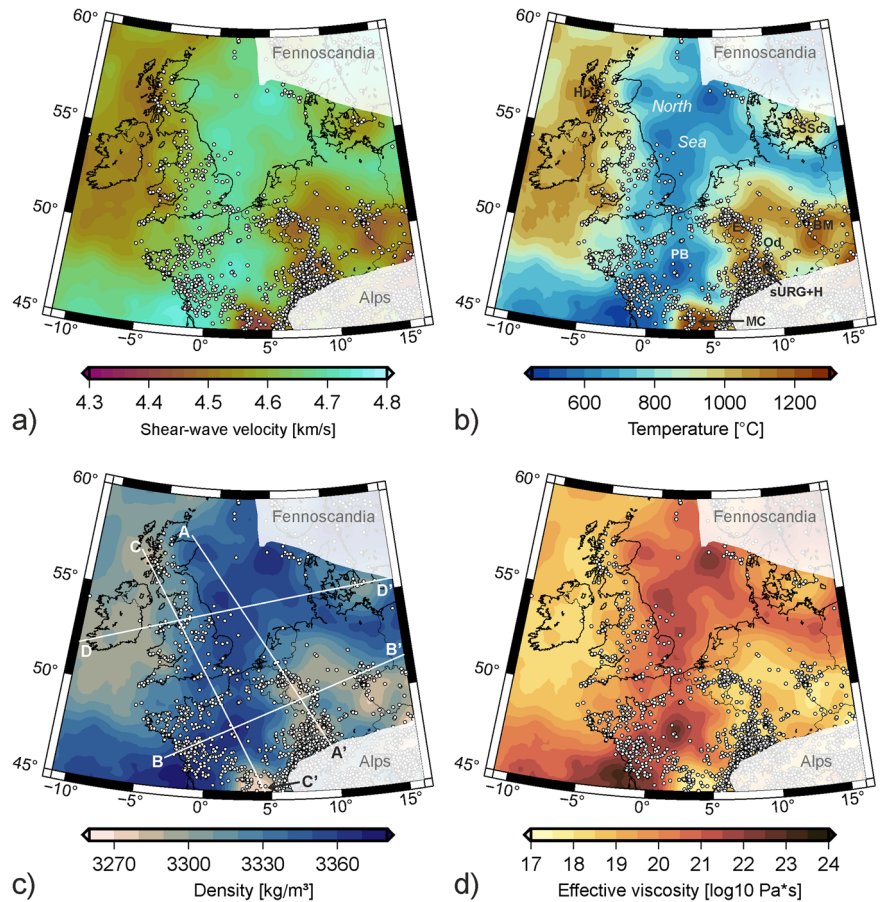
The main finding of this study is that seismicity is (i) largely limited to regions that exhibit a low-density layer in the uppermost lithospheric mantle and (ii) preferentially clustered above lateral gradients in upper mantle effective viscosity. We propose that these spatial correlations reflect the importance of buoyancy forces within the mantle lithosphere in this low-strain intracontinental setting. As an additional factor, the forces due to gravitational instabilities, plate tectonics, and GIA seem to interact with mantle strength heterogeneities and thus localize mantle deformation and related differential loading of the overlying crust. With this mantle perspective on earthquake distribution, our study provides new clues concerning the differentiation of the study area into seismically quiet regions (e.g., Ireland, Paris Basin) and elongated zones of increased seismicity (e.g., mainland Britain, Rhine Graben system).

## Results

We have extracted the depth to the 1300 °C isotherm from the  $v_s$ -tomography-derived temperature configuration as a proxy for variations in the depth of the lithosphere-asthenosphere boundary (LAB) across western and central Europe (Fig. 2). Accordingly, the largest lithosphere thicknesses ( $>180$  km) are present beneath the southwestern North Sea and Paris Basin regions which overall show lower seismic activity than regions of thinner ( $<140$  km) lithosphere to the east and west.

At intra-lithospheric depth of 80 km, the mantle reveals three major anomalies of low velocity, high temperature ( $>1000$  °C) and correspondingly low density and effective viscosity (Fig. 3): the western British Isles with the strongest anomaly below the Hebrides, an anomaly offshore southernmost Scania, and the NW foreland of the Alps with highest temperatures below the Massif Central, the southern Upper Rhine Graben-Hegau region, the Eifel, and the NW Bohemian Massif. Temperature lows beneath the southwestern North Sea, the Paris Basin, and the Odenwald area bound these positive mantle thermal anomalies and reveal comparatively little seismic activity. In general, the majority of seismic events tend to align above the boundaries of relative thermal highs and lows in the upper mantle. For

**Fig. 3 | Characteristics of the lithospheric mantle at a depth of 80 km.** **a** Shear-wave velocity as taken from the full-waveform inversion derived model CSEM Europe<sup>14</sup>; **b** temperature; **c** density with locations of the profiles shown in Fig. 4–7; **d** effective viscosity. White dots are hypocenter locations of the ESHM20 seismic catalog<sup>3</sup>. Abbreviations for mantle thermal anomalies in **b**: BM Bohemian Massif, E Eifel, Hb Hebrides, MC Massif Central, Od Odenwald, PB Paris Basin, SSca Southern Scania, sURG+H southern Upper Rhine Graben and Hegau region.



example, a broad N-S striking earthquake belt from Scotland to SW England and further to the South Armorican Seismic Zone in France is located above the western flank of the colder lithospheric keel (Fig. 2). East of the keel (in the ECRIS), seismicity clusters and belts are generally narrower, such as along the Rhine Graben sections, and they seem to avoid the centers of positive and negative mantle thermal anomalies (e.g., Eifel, Odenwald; Fig. 3b). Finally, earthquakes above the keel are limited to two narrow belts: one above a NW-SE striking LAB bulge from southeast England to the Netherlands (Fig. 2) and a second one above a NE-SW striking, positive thermal anomaly in the shallow lithosphere across northern France (Fig. 3b).

To discuss the lateral distribution of seismic events also in the light of vertical mantle structure, we present the  $v_s$ -derived parameters (temperature, effective viscosity, density) along four transects, two roughly parallel to  $S_{Hmax}$  (running NW-SE) and two perpendicular to the strike of the lithospheric keel (for locations see Fig. 3c). Profile A runs from the North Sea towards the northern Alpine Deformation Front and highlights the depth variations in the thermal LAB, which reaches >200 km in the north and locally <120 km in the south (Fig. 4). While the North Sea domain is essentially free of natural seismicity, three earthquake clusters are recorded further south, associated with the Lower Rhine Graben (LRG), the Upper Rhine Graben (URG), and the Alpine Deformation Front (ADF). At shallow mantle depths (<100 km), the high-temperature-low-viscosity domains of the Eifel and the southern Upper Rhine Graben-Hegau region are situated below seismically quiet crust separating the previously mentioned earthquake clusters. Furthermore, at intralithospheric depths of 50–120 km, the high-temperature anomalies appear as distinct density lows. Actually, it is above the sub-vertical boundaries of these density minima where crustal seismicity is concentrated.

Profile B shows crust and upper mantle structures from the Armorican Shelf in the SW to the Northeast German Basin in the NE (Fig. 5). The

eastern half of the transect is dominated by a sub-lithospheric positive thermal anomaly (>1300 °C) that splits above into two domains of hot lithosphere, namely the Eifel and the Bohemian Massif anomalies. Similar to Profile A, the main seismic zones (i.e., the Northern Upper Rhine Graben and Leipzig-Regensburg-Seismic Zone) are laterally offset with respect to the hottest domains in the shallow mantle (<120 km) and located above sub-vertical bounds of the corresponding density lows (Eifel, Bohemian Massif). Towards the Odenwald and Paris Basin regions, in contrast, seismic activity is considerably reduced. The Paris Basin also stands out from the transect due to its lithospheric mantle density that is continuously increasing downwards (like below the southern North Sea; Fig. 4), which is in contrast to a low-density layer within the uppermost mantle below the South Armorican Seismic Zone.

Profile C connects the positive mantle thermal anomalies of the Hebrides in the NW and the Massif Central in the SE (Fig. 6), thus imaging seismicity above a range of lithosphere thicknesses and including the two narrow belts of seismicity above and across the lithospheric keel. Even more remarkable than the LAB geometry, however, is the complexity of the intralithospheric thermal and density configuration. While at depths of >120 km, the cold, stiff and high-density mantle domain stretches from the Paris Basin far north into SE England, at 50–80 km depth the  $v_s$ -tomography indicates a narrow high-temperature-low-density anomaly below the Eastern Channel, the lateral bounds of which are overlain by two isolated clusters of seismicity. While the LAB depth decreases gradually towards the NW, there are distinct lateral mantle density contrasts—and locally even domains of downward decreasing density—within the mantle lithosphere, just below the seismically active zones of mainland Britain.

Profile D runs from Ireland across mainland Britain towards the Baltic Sea and images a pronounced asymmetry in the North Sea portion of the lithospheric keel in terms of both crustal seismicity as well as upper mantle configuration (Fig. 7). Despite similar LAB depths ( $150 \pm 20$  km) to the west

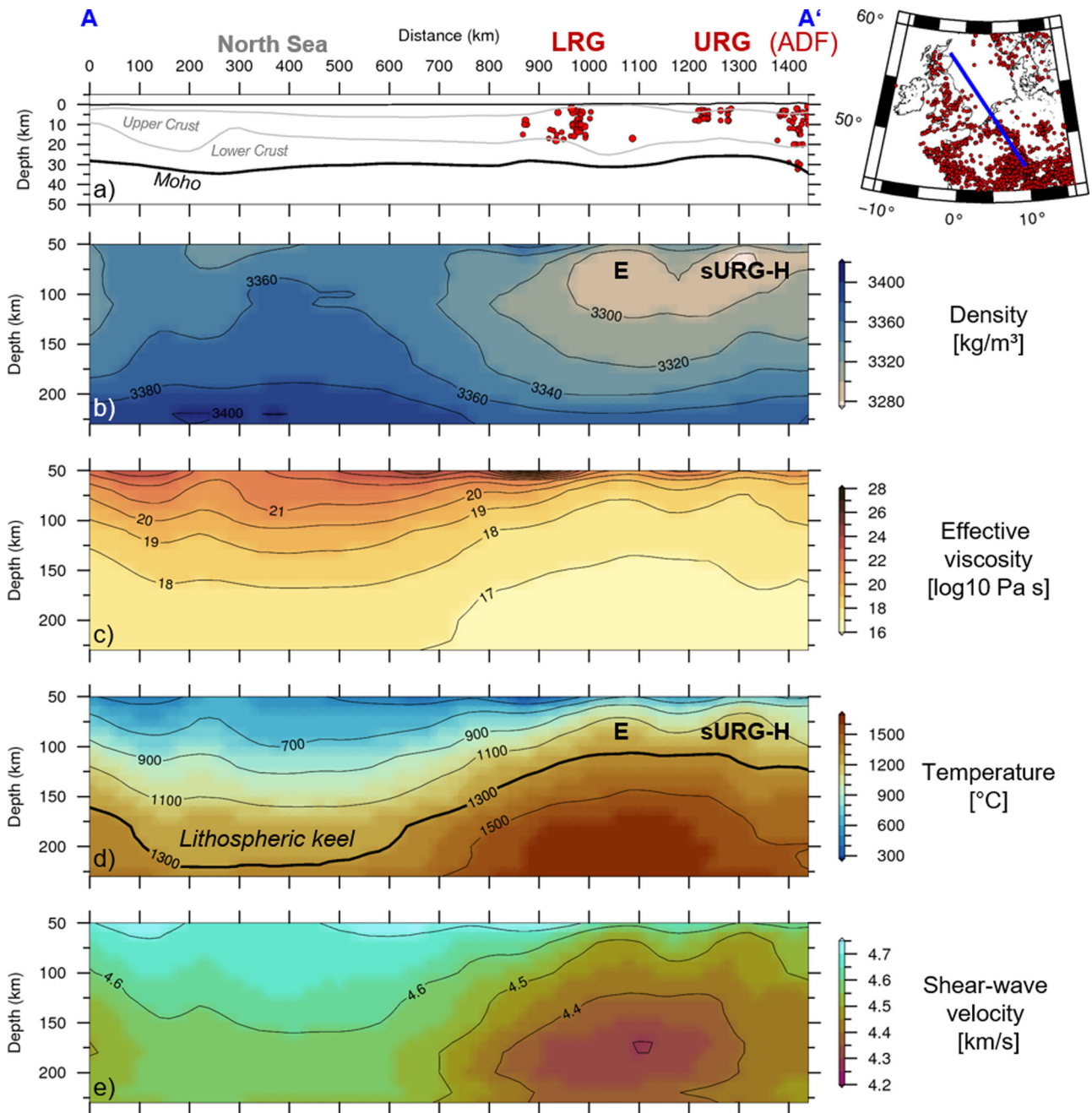


**Fig. 4 | Profile A transecting the crust and upper mantle from the southern North Sea to the Alps.** For location of A-A' see also Fig. 3c; a crustal structure (EuCrust07 model<sup>85</sup>) with hypocenters of the ESHM20 catalog<sup>7</sup> located at a perpendicular distance of <15 km from the profile. Mantle density (b), effective viscosity (c), and

temperature (d) are derived from shear-wave velocity (e CSEM Europe<sup>14</sup>). Clusters of seismicity: ADF Alpine Deformation Front, LRG Lower Rhine Graben, URG Upper Rhine Graben; mantle thermal anomalies: E Eifel, sURG+H southern Upper Rhine Graben and Hegau region.

and east of the keel, the temperature and density configurations in the shallower lithospheric mantle are significantly different: in the west, a horizontally stratified configuration of downward increasing mantle density below a seismically quiet crust in Ireland translates into a more variable mantle structure with downward decreasing density beneath a seismically active crust in England. In contrast, there is a more gradual temperature and density distribution across and beyond most of the eastern flank of the keel where, overall, less seismic activity is recorded.

**Discussion**

Interpreting  $v_s$ -anomalies as narrow as a few hundred kilometers, imaged by a continental-scale mantle tomographic model, raises questions concerning their reliability. A great share of our confidence in the existence and location

of the lithospheric keel (Fig. 2) is based on the fact that the respective long-wavelength variations in upper mantle  $v_s$  imaged by CSEM Europe<sup>14</sup> are consistent with previously published global and regional tomography models<sup>15-18</sup>. Likewise, global models of lithospheric thickness derived from  $v_s$ -tomographic models<sup>19,20</sup> are also consistent with the obtained first-order trend in the LAB geometry across the study area. In addition, seismology-independent indications for the presence of a distinct high-density anomaly in upper mantle reaching from the southern North Sea to north-central France come from co-located lows in upper mantle geoid models<sup>21,22</sup> (see also Supplementary Fig. 1d in the Supplementary Discussion).

CSEM Europe<sup>14</sup> also reproduces smaller-scale anomalies inside the mantle lithosphere, identified in dedicated local studies, remarkably well. A recently published surface wave tomography, for instance, reveals a N-S belt

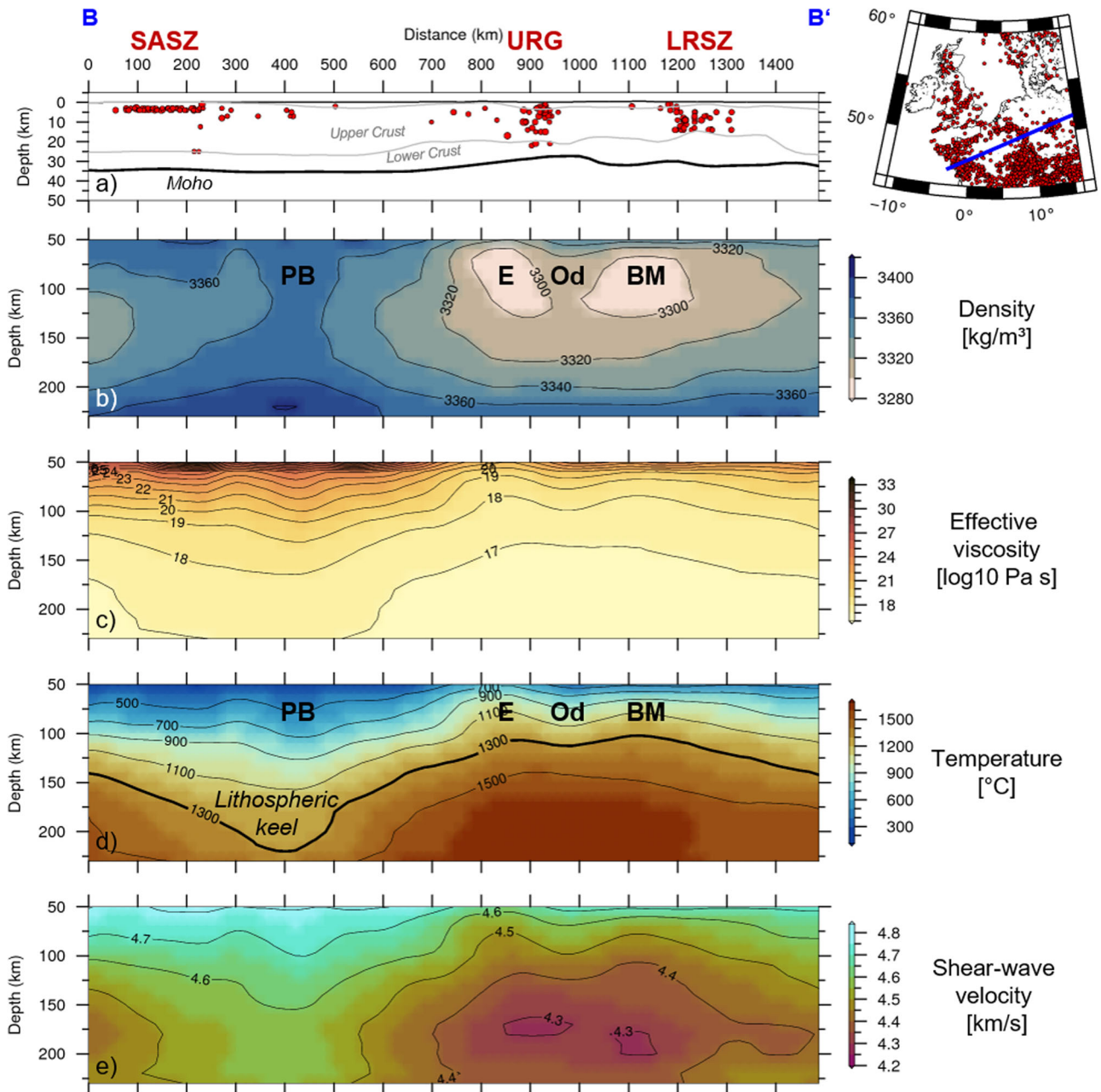


**Fig. 5 | Profile B transecting the crust and upper mantle from the Bay of Biscay to the Northeast German Basin.** For location of B-B' see also Fig. 3c; a crustal structure (EuCrust07 model<sup>85</sup>) with hypocenters of the ESHM20 catalog<sup>3</sup> located at a perpendicular distance of <50 km from the profile. Mantle density (b), effective viscosity

(c), and temperature (d) are derived from shear-wave velocity (e; CSEM Europe<sup>14</sup>). Clusters of seismicity: LRSZ Leipzig-Regensburg Seismic Zone, SASZ South Armorican Seismic Zone, URG Upper Rhine Graben; mantle thermal anomalies: BM Bohemian Massif, E Eifel, Od Odenwald, PB Paris Basin.

of negative phase-velocities at depths of 60–130 km located between Ireland and eastern mainland Britain<sup>11</sup>, which corresponds well in extent with the low- $v_s$ -high-temperature domain at c. 80–150 km imaged by CSEM Europe<sup>14</sup> (“IRS” in Fig. 7; see also Supplementary Fig. 1). Likewise, a teleseismic traveltime-derived P-wave velocity model<sup>23</sup> supports the general trend of increasing velocities from western to eastern mainland Britain. Further to the east, the shallow-mantle, high-temperature anomaly offshore Scania imaged by CSEM Europe<sup>14</sup> (Fig. 2b) stretches to the NW at larger depths (e.g., 150 km; Supplementary Fig. 1b), which agrees well with the configuration of a low P-wave velocity anomaly imaged by a local traveltime tomography<sup>24</sup>. Similarly, low- $v_p$  anomalies in the upper mantle of the Eifel region<sup>25</sup> and the Massif Central<sup>26</sup>—both interpreted as originating from mantle plumes—coincide in size and position with low- $v_s$  domains in CSEM Europe<sup>14</sup> (Fig. 3b). Additionally, the main pattern of uppermost

mantle P-wave velocity across the Bohemian Massif<sup>27</sup> is reproduced by CSEM Europe<sup>14</sup> in that the outer and northwestern parts of the massif mainly show negative  $v_s$ -anomalies, while in the south-central parts high-S-wave velocity perturbations prevail (Fig. 3b). Finally, according to CSEM Europe<sup>14</sup>, the shallowest mantle high-temperature anomaly beneath the Upper Rhine Graben-Hegau region (Fig. 2b) turns into a low-temperature domain at depths of >120 km (Fig. 4; Supplementary Fig. 1b)—which is in contrast to the Eifel and the NW Bohemian Massif anomalies that are vertically connected to a deeper hot domain, but in agreement with local P-wave velocity tomographic models of the southern Upper Rhine Graben<sup>28</sup>.

Our conversion results reflect the method-inherent, non-linear relationships between  $v_s$  and derived temperature, respectively density. This becomes obvious, for example, from the transects through the Alpine

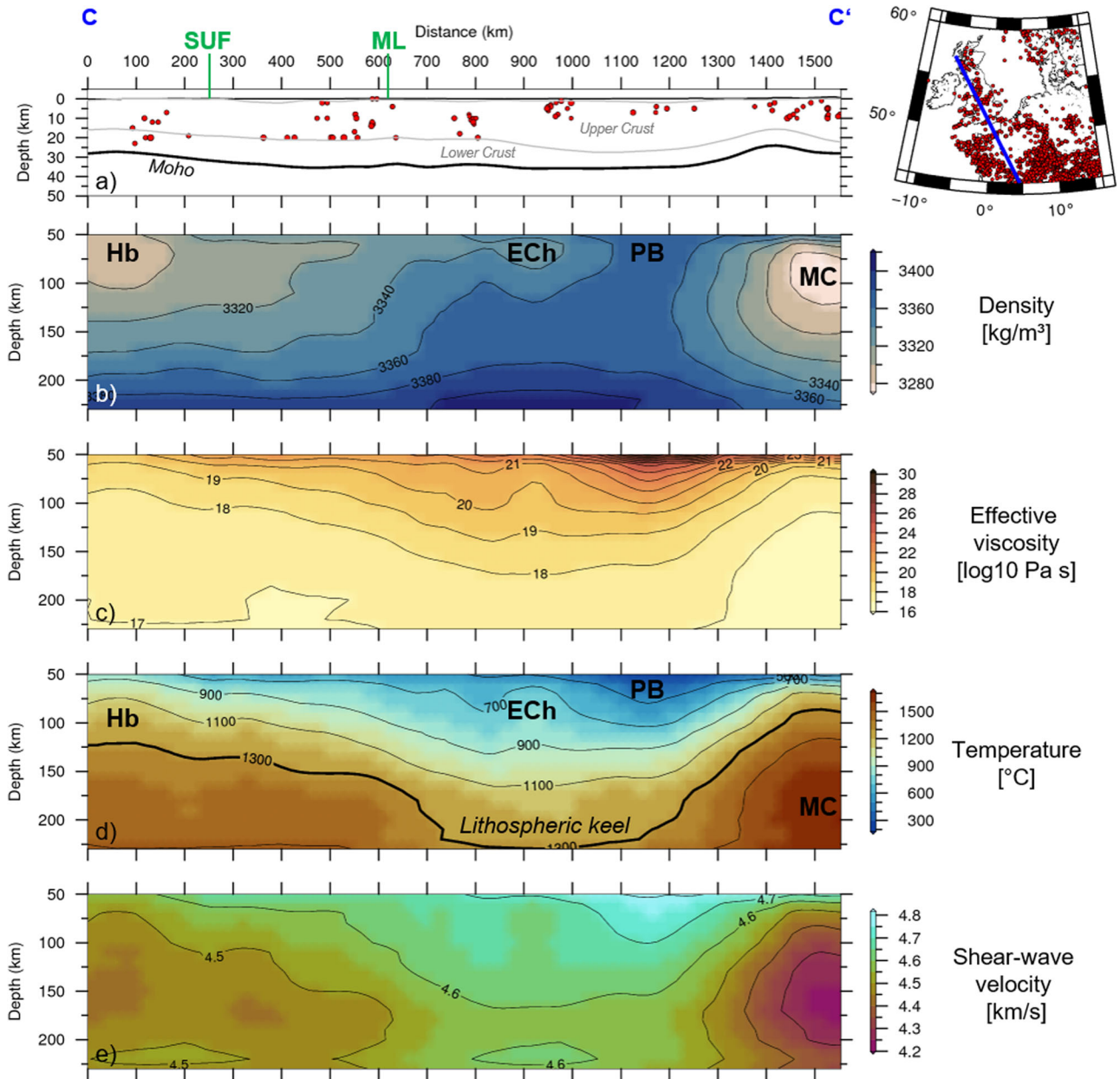


**Fig. 6 | Profile C transecting the crust and upper mantle from the Hebrides to the Massif Central.** For location of C-C' see also Fig. 3c; a crustal structure (EuCrust07 model<sup>85</sup>) with hypocenters of the ESHM20 catalog<sup>3</sup> located at a perpendicular distance of <50 km from the profile. Mantle density (b), effective viscosity (c), and

temperature (d) are derived from shear-wave velocity (e; CSEM Europe<sup>14</sup>). Crustal sutures: ML Malvern Line<sup>92</sup>; SUF Southern Uplands Fault<sup>86</sup>; mantle thermal anomalies: ECh Eastern English Channel, Hb Hebrides, MC Massif Central, PB Paris Basin.

foreland, where  $v_s$  minima are located at larger mantle depths than the respective density minima (Figs. 4 and 5) and confirms our strategy of converting the seismological model before interpreting it with respect to its potential relation to seismicity. These across-depth insights into the upper mantle physical configuration are facilitated by the applied conversion approach which derives bulk rock properties for mineralogical compositions that are strictly thermodynamically stable in the given, wide range of pressure and temperature conditions possible in the upper mantle (see Methods). The observation that earthquakes preferentially occur in clusters and belts above large lateral gradients in the derived temperature and density variations of the upper mantle (e.g., Fig. 3) raises the question of potential causal relationships between mantle anomalies and seismic stress release in the overlying crust, which will be discussed in the remaining parts of this section.

Deep drilling experiments and fluid-injection induced seismicity provide evidence that large parts of the brittle crust in the study area are critically stressed<sup>29</sup> so that earthquakes potentially can be triggered wherever even smallest, transient stress (or fault strength) perturbations release elastic energy from this tectonically or thermally loaded lithosphere<sup>1</sup>. Fault plane solutions and the respective directions of  $S_{Hmax}$  in the study area are consistent with the plate boundary forces induced, background tectonic stress field, which has been proposed to be typical for the diffuse seismicity in low-strain continental plate interiors<sup>1</sup>. In view of the low strain rates, however, the question arises as to which type of transient, non-tectonic process is capable of triggering the earthquakes. A classical candidate would be the sudden establishment of pore fluid overpressure which decreases the effective normal stress on fault planes and thus reduces slip resistance. The importance of this mechanism for fault reactivation in the intraplate New

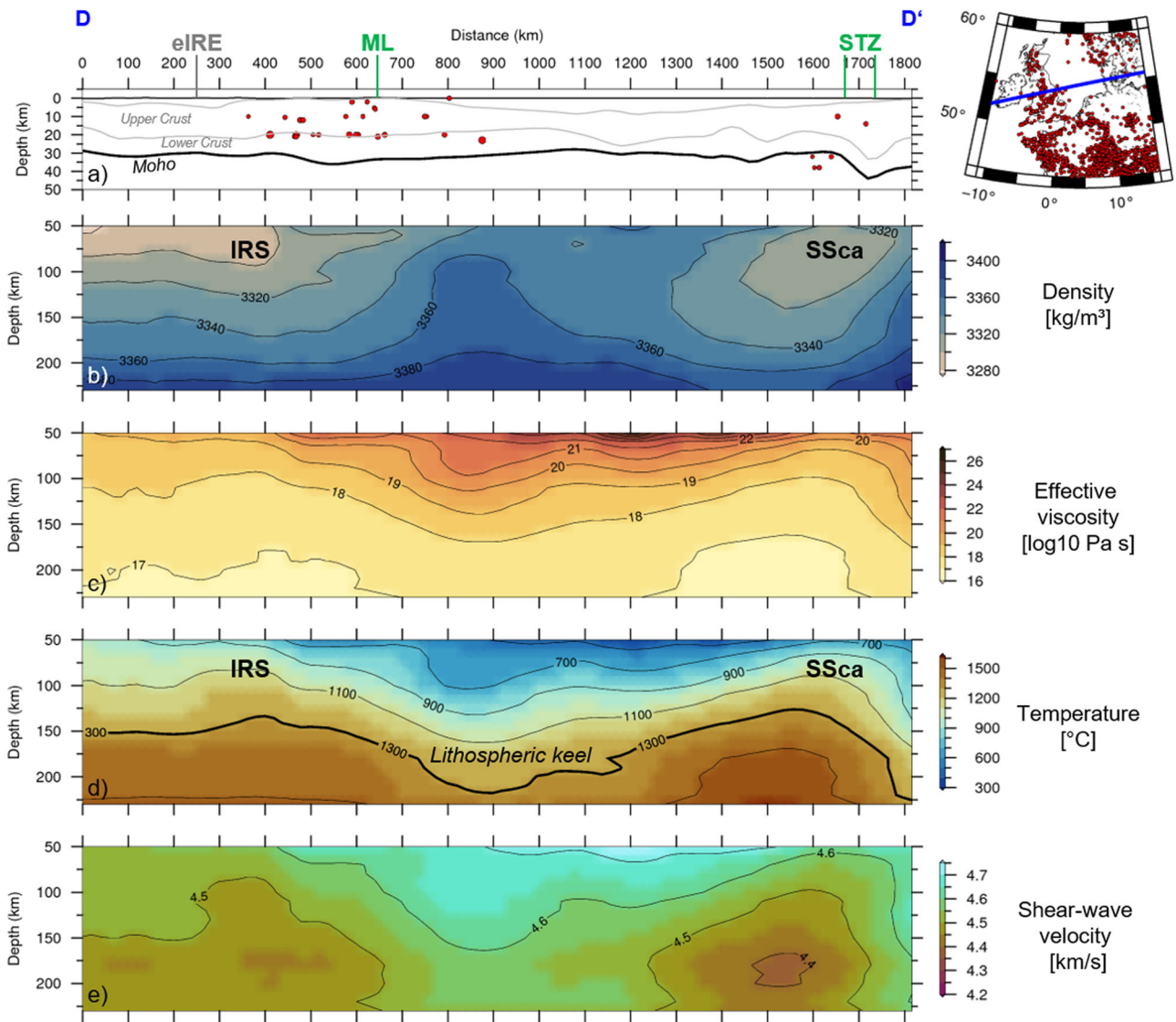


**Fig. 7 | Profile D transecting the crust and upper mantle from Ireland to the western Baltic Sea.** For location of D-D' see also Fig. 3c; **a** crustal structure (EuCrust07 model<sup>85</sup>) with hypocenters of the ESHM20 catalog<sup>3</sup> located at a perpendicular distance of <50 km from the profile. Mantle density (**b**), effective viscosity

(**c**), and temperature (**d**) are derived from shear-wave velocity (**e**; CSEM Europe<sup>14</sup>). eIRE east coast of Ireland; crustal sutures: ML Malvern Line<sup>92</sup>, STZ Sorgenfrei-Tornquist Zone; mantle thermal highs: IRS Irish Sea, SSca Southern Scania.

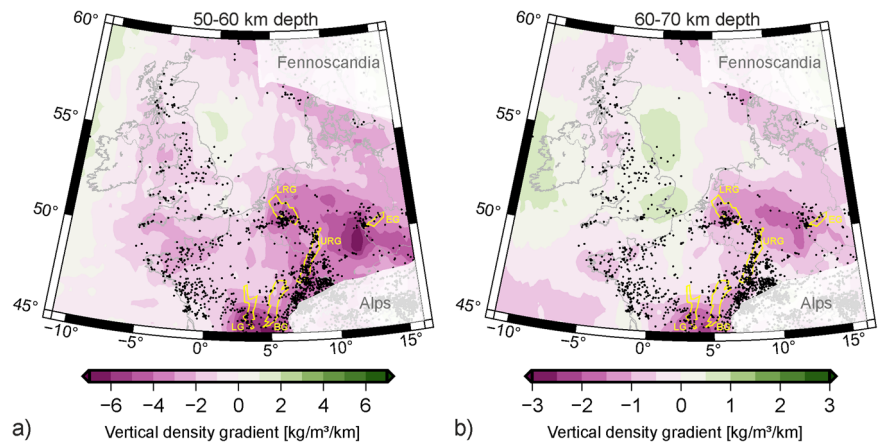
Madrid Seismic Zone has recently been demonstrated by means of a Mohr-Coulomb-model based parametric analysis for a wide range of stress-state/fault-friction scenarios<sup>30</sup>. In western and central Europe, gas emanations observed above the Massif Central, the Eifel and the NW Bohemian Massif mantle anomalies prove that mantle fluids locally reach the Earth's surface<sup>31</sup> with the potential for mechanically affecting the subsurface on their way up. Furthermore, a causal relationship between mantle-derived fluid flow and the initial triggering of local earthquake swarms has been proposed for the Leipzig-Regensburg Seismic Zone<sup>32,33</sup>. However, evidence for a causal relation between subsurface fluid flow and natural earthquakes is spatially very restricted and thus cannot be used as an overall explanation for the seismicity distribution across the study area.

Like in plate boundary settings, intraplate seismicity is facilitated by the presence of mechanical discontinuities, such as pre-existing faults and fracture zones, that are weaker than the hosting rock<sup>34</sup>. Indeed, major Paleozoic fault zones of the British Isles have been suggested to exert control on the localization of individual seismic events<sup>35</sup>; the same tectonic elements, however, can be traced all the way to Ireland, where they are part of a seismically inactive crust, thus putting the interpretation of a primary fault

control in question. Likewise, in metropolitan France there is a trend of increased earthquake frequency around crustal-scale fault zones, but this correlation does not hold for the Paris Basin region<sup>36</sup>. For northern Germany, Late Cretaceous inversion structures have been identified as localizing elements for seismicity<sup>7</sup>. However, regions of abundant seismic activity in Germany have been found to rarely coincide with regions that accumulated higher strain over the various tectonic periods as indicated by multiple fault reactivation in the past<sup>37</sup>. Hence, although pre-existing crustal weaknesses can be a contributive factor under favorable stress conditions, the reactivation of such elements cannot explain the first-order trends in the presence and absence of seismicity across the entire study area.

Differential stresses in the crust can be sourced in the lithospheric mantle where proper mechanical connections between ductile and brittle parts of the plate exist. This seems to be applicable in Australia where mantle attenuation patterns spatially correlate with earthquake clusters, indicating that higher strain rates within mantle domains of low viscosity increase differential stresses and thus seismicity in the overlying crust<sup>12</sup>. For western and central Europe, the heterogeneities in effective viscosity as derived from the converted mantle temperature distribution (Fig. 3d), first of all indicate

**Fig. 8 | Downward decreasing density as a proxy for buoyancy related gravitational instabilities in the shallow upper mantle below zones of increased seismicity.** For the depth intervals of 50–60 km (a) and 60–70 km (b), the integrated mean vertical density gradients have been derived from the  $v_s$ -converted density configuration. Negative values (violet) indicate downward decreasing density. The deeper the interval, the more common are positive values (green) representing downward increasing density. Black dots mark hypocenters of seismic events (ESHM20 catalog<sup>3</sup>). Grabens of the ECRIS<sup>90</sup> (yellow) are shown for orientation. BG Bresse Graben, EG Eger Graben, LG Limagne Graben, LRG Lower Rhine Graben, URG Upper Rhine Graben.



non-uniform stress-strain relations in the upper mantle. These viscosity contrasts generally increase upwards and are strongest close to the crust-mantle boundary (Figs. 4–7). They may be even more pronounced where strain rates in reality peak, which in our model is implicitly prevented through the constant-strain-rate assumption (Methods). The fact that we find seismic activity in western and central Europe to be concentrated above large lateral upper mantle temperature gradients may reflect differential stresses imposed on the crust to be enhanced above the transitions between rheologically weaker and stronger mantle domains. This would be consistent with 3D finite element models showing that localized viscoelastic relaxation in the mantle imposes differential stresses on the crust large enough to explain the earthquake distribution of the New Madrid Seismic Zone<sup>38</sup>. In contrast, upper mantle domains of lowest viscosity as the Eifel anomaly are overlain by a seismically less active crust, which may indicate that kinetic energy is efficiently dissipated by viscous (aseismic) deformation there, effectively unloading the brittle domain. Moreover, regions with continuously high effective viscosity as the southern North Sea and Paris Basin (Figs. 2 and 3d) may simply accumulate too little strain in the upper mantle to contribute to intensive seismic deformation in the crust.

Another potential source of differential stresses imposed on the brittle domain may be given by mantle intrinsic density-related forces. First of all, the  $v_s$ -tomography-derived lateral density gradients (Fig. 3c) imply variations in gravitational potential energy (GPE) originating in the upper mantle and involving horizontal compressional forces from high-density domains exerted on low-density domains. Interestingly, the first-order pattern of the inferable variation in GPE is consistent with undulations in modeled upper mantle components of the geoid<sup>22</sup> (Supplementary Fig. 1d), thus indicating that density variations are gravitationally effective. If the corresponding horizontal forces are locally large enough to contribute to an activation of mantle relative displacements, this would provide an additional explanation for clustered seismicity above large lateral temperature gradients. In this way, we follow the arguments of a previous study suggesting that such short-wavelength density heterogeneities in the upper mantle of the central and eastern United States would decisively affect the lithospheric GPE and thus explain the distribution of intracontinental seismicity there<sup>39</sup>.

A second type of mantle intrinsic force is revealed by the tomography conversion in the form of low-density bodies in the shallowest lithospheric mantle, surrounded and overlain by higher-density material (Fig. 4–7) and thus implying buoyancy forces that act against gravity. To tentatively map variations in these forces across the entire study area, we take advantage of the downward decreasing density at the top of these low-density structures and plot the vertically integrated average density gradient ( $\bar{\rho}_z$ ) for each geographic position. For the depth intervals of 50–60 km and 60–70 km, we find that actually all seismic events are located above negative values of  $\bar{\rho}_z$  and seismicity is more concentrated above larger negative values, respectively large horizontal gradients in  $\bar{\rho}_z$  (Fig. 8). Provided that these vertical gradients are indeed a measure for mantle intrinsic buoyancy forces, we can

infer gravitational instabilities in the shallowest mantle to contribute to favorable conditions for seismicity across much of the study area. Note that downward decreasing densities only occur where vertical thermal gradients in the shallowest mantle are large enough so that the effects of thermal expansion outweigh those of pressure-driven compressibility, the latter increasingly dominating towards greater depths<sup>40</sup>. Such pressure-temperature conditions leading to inverse density gradients are widely prevalent in the ECRIS with its early Cenozoic to recent volcanic fields and distributed seismicity (Figs. 4 and 5). In contrast, subregions that mainly reveal downward increasing mantle densities (positive  $\bar{\rho}_z$ )—such as the southern North Sea (Fig. 4), the Paris Basin (Fig. 5) and Ireland (Fig. 7)—show very little or no seismic activity (Fig. 8).

External sources of energy usually discussed to be responsible for differential stresses in the lithosphere also include mantle convection and related shear tractions at the LAB. Numerical mantle flow models, for example, indicate that the rate change of vertical normal stress induced by mantle flow at the transition from thin to thicker lithosphere is the most important controlling factor for seismicity clustering in the western United States<sup>41</sup>. Likewise, a lithospheric keel beneath the Great Artesian Basin (Australia) oriented at high angle to the northward motion of the plate is suggested to increase shear tractions exerted by the southward sublithospheric flow to the lithosphere base and horizontal tectonic stresses in the resisting plate and thus may lead to seismicity rates growing from the northern towards the southern Great Artesian Basin<sup>42</sup>. For western and central Europe, global convective models show that sublithospheric mantle flow would induce very low dynamic topography<sup>43</sup>; on the other hand, these models reveal that flow has been directed roughly from west to east over the past 50 Myr until present. Accordingly, we can infer that low-viscosity material collides at a large angle with the western, more steeply dipping flank of the lithospheric keel (Figs. 2 and 6). If such mechanical lithosphere-asthenosphere interactions are strong enough for the related stresses to be effectively transmitted into the seismogenic zone, this may explain why the largest number of earthquakes in mainland Britain and western France occur right above the transition between thinnest and thickest lithosphere (Figs. 2 and 7).

Turning to the top of the lithosphere, stress-strain relationships in western and central Europe are proposed to result at least locally from the adjustment of a visco-elastic lithospheric plate to the waxing and waning of ice sheets<sup>5</sup>. Considering the time elapsed since the latest glaciations in this part of Europe (~10–15 kyrs), any vertical movements induced by GIA would rather reflect the viscous tail of the viscoelastic response of the lithospheric plate to ice retreat. Therefore, the timing and magnitudes of associated uplift would be dictated by the viscosity configuration of the rigid mantle and heterogeneities therein. The spatial correlations between tomography-derived temperature-driven upper mantle instabilities and earthquake clusters indicate that these intra-lithospheric heterogeneities indeed provide a first-order contribution to ongoing (partly deglaciation

controlled) deformation. It is not possible, however, to determine what proportion of the resulting strain is due to post-glacial rebound. Given that we are looking at the end results of a coupled and non-linear dynamic system, in general, a clear distinction between external and internal forces on the lithosphere would require to model the transient effects of glacial loading and isostatic response.

Although our findings suggest that deformation in the mantle and seismicity in the crust are mechanically linked, a more detailed understanding of this connection is still missing. Based on observations from fault systems in different orogens and rifts, it has been proposed that recurrent seismicity is generally associated with deeper domains of long-term weakness and that earthquakes could be even used to locate the active parts of long-lived, deep-seated (mantle) shear zones<sup>44</sup>. The shallow to deep lithospheric connection in various tectonically active regions is also reflected by post-earthquake motions. These can be causally related to viscoelastic relaxation (if the temporal coverage of related measurements is broad enough) and thus even allow to derive upper mantle viscosity beneath the seismogenic zone<sup>45</sup>. Now conversely viewed, can also ductile deformation zones in the lithospheric mantle localize the triggering of crustal earthquakes? In the study area, the tomography-derived domains of buoyant upper mantle at least do not consistently match in location and extent with regions of surface uplift as indicated by GNSS-derived velocity field models<sup>2</sup>; some low-density mantle anomalies as those under the Massif Central or Upper Rhine Graben are even overlain by currently subsiding crust. This raises questions not only concerning the effective mechanisms causing across-depth deformation but also regarding the thermodynamic evolution of this dissipative system in which, for example, present-day positive thermal anomalies may currently undergo cooling, involving subsidence at the surface. Moreover, although tensional deviatoric stress states dominate above the mantle anomalies of the Eifel and the Massif Central suggesting a mantle-driven bulge of the crust there<sup>46</sup>, the remaining parts of the study area show extensional, compressional and strike-slip faulting regimes alternating over much smaller distances<sup>4</sup> than the wavelengths of obtained upper mantle anomalies. Given furthermore that the majority of analyzed focal mechanisms imply a very uniform  $S_{Hmax}$ , we conclude that it is not the kinematics of seismogenic faults but the locations of their active parts that actually reflect localized mantle deformation.

To shed light onto mechanisms sourced in the mantle that could cause crustal seismicity in this intracontinental setting, it would be essential to develop continuous rheological models from the convective parts of the mantle across all potential brittle-ductile transitions into the seismogenic zone. An important question to answer thereby would be how mantle dynamics operating at time scales of millions of years and potentially involving dissipative processes (such a shear heating or grain growth healing) could lead to seismic stress release in the crust over seconds to days. It has been shown that continuous water draining in ductile shear zones of the upper mantle can provide important fluid reservoirs potentially also impacting on the fluid distribution in the crust<sup>47</sup>. Therefore, we may finally put up for further discussions whether a sudden achievement of some (yet unknown) critical mantle fluid pressure could mark the start of a chain of coupled thermal-hydraulic-mechanical processes that finally trigger crustal earthquakes even without any mantle fluids rising all the way up to the Earth's surface and thus even in regions where we are lacking crustal evidence for mantle derived fluids.

## Conclusions

Inspired by some obvious spatial correlations in intracontinental western and central Europe between shear-wave velocity anomalies in the upper mantle and seismicity clusters in the overlying crust, we have converted<sup>48</sup> tomographic seismic velocity to temperature (indicative for effective viscosity) and density. This is our attempt to quantitatively elaborate on how a heterogeneous density and viscosity configuration in the lithospheric mantle may affect crustal deformation. While we still have to remain speculative concerning the underlying mechanisms at this stage, our findings clearly support the hypothesis that upper mantle thermal

anomalies affect the distribution of earthquakes across the region. We can even attempt to draw some conclusions on the relative importance of different seismicity controlling factors in different parts of the system. It is west of the lithospheric keel, just above the transition from thinnest to thickest lithosphere, where the broad belt of seismicity from mainland Britain to western France may indicate that basal tractions imposed by eastward asthenospheric flow may contribute to crustal deformation. Variations in the depth of the thermal LAB and thus overall lithospheric strength, in contrast, seem to be less decisive for the lateral distribution of events all across the study area. What is common to all seismically active subregions and thus seems to be the primary mantle source of differential stresses, however, is the presence of low-density domains situated in the shallow mantle, right below material of higher mantle density, and thus imposing buoyancy forces onto the nearby crust. Such gravitational instabilities inside the mantle lithosphere provide an explanation for seismicity to occur even in areas of thickest (coldest and thus strongest) lithosphere, such as around the Eastern English Channel. On the other hand, for regions with mantle density dominantly increasing downwards—like beneath Ireland, the southern North Sea and the Paris Basin—the lack of intrinsic mantle buoyancy forces provides an alternative to previous explanations for the reduced seismicity there<sup>49</sup>. According to both the configuration of buoyant low-density anomalies in the upper mantle (Fig. 8a) and lateral mantle density and GPE gradients (Fig. 3c), the effects of intrinsic mantle forces are strongest east of the lithospheric keel, across the ECRIS. There, our results may also shed new light on the enigmatic 90°-turn of the graben structures and related seismicity belt from the Upper Rhine Graben into the rheologically stronger crust hosting the Lower Rhine Graben<sup>50</sup> (Fig. 8). We propose that the present deformation in the Lower Rhine Graben is affected by stress and strain concentrations induced by mantle displacements which, in turn, are a response to (i) the buoyant shallow-mantle domain of strongly downward decreasing density (Fig. 8a) and (ii) the lateral strength contrasts around the nearby, low-viscosity mantle anomaly of the Eifel (Fig. 3d).

In conclusion, we propose that plate boundary and GIA-related forces interact with mantle intrinsic buoyancy forces to destabilize the lithospheric plate in this intracontinental setting. The  $v_s$ -tomography derived mantle temperature configuration furthermore reveals how this plate would respond, i.e., where these forces at interplay with mantle strength heterogeneities most likely would induce displacements in the lithospheric mantle capable of causing increased seismicity in the overlying, prestressed crust.

## Methods

For the conversion of the mantle  $v_s$ -model to thermodynamically consistent temperature and density configurations, we use V2RhoT\_gibbs<sup>48,51</sup>. This open-source Python application performs conversions based on pre-computed look-up tables of pressure and temperature-dependent seismic velocity (Fig. 9). These look-up tables, in turn, are generated using the module Generator\_LINUX of LitMod2D\_2.0<sup>52,53</sup>, which applies a Gibbs-free energy minimization algorithm (Perple\_X algorithm<sup>54,55</sup>) for a given bulk mantle chemical composition in terms of weight-% of major oxides (the Na<sub>2</sub>O-CaO-FeO-MgO-Al<sub>2</sub>O<sub>3</sub>-SiO<sub>2</sub> system accounting for ~99% of the Earth's mantle<sup>56</sup>). Using V2RhoT\_gibbs<sup>48,51</sup>, the algorithm determines the stable state in terms of phase and mineral assemblages based on an augmented and modified version<sup>57</sup> of an original thermodynamic database<sup>58</sup>. Thereby, pressure is approximated as lithostatic load using the density information of a reference model<sup>53</sup> seismically equivalent to the standard seismological ak135 model<sup>59</sup>.

As an additional component of V2RhoT\_gibbs<sup>51</sup>, precomputed anharmonic values of  $v_s$  are corrected for anelastic attenuation effects according to a set of empirical equations<sup>60</sup>. Therefore, we have set the assumed grain size for the mantle material equal to 10 mm and the wave oscillation period to 75 s (as this combination matches well global attenuation models at depth levels around the LAB<sup>53</sup>). In addition, V2RhoT\_Gibbs<sup>51</sup> corrects shear-wave velocities for the effects of partial melts using an empirical relation<sup>61,62</sup>, while integrating an indicative melt

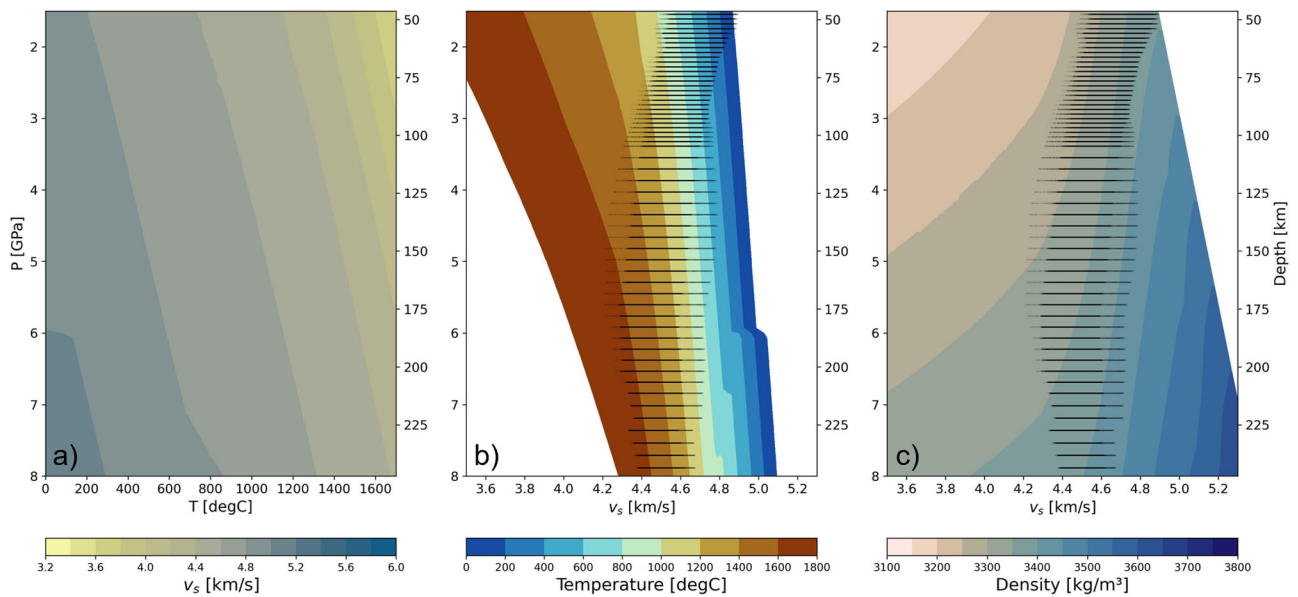


**Fig. 9 | Conversion of shear-wave velocity to temperature and density.** The predefined mantle chemical composition Pr\_1<sup>71</sup> used here includes 44.7% SiO<sub>2</sub>, 2.1% Al<sub>2</sub>O<sub>3</sub>, 7.9% FeO, 42.4% MgO, 1.9% CaO, 0.15% Na<sub>2</sub>O (Mg#=90.6). **a**  $v_s$  as a function of pressure and temperature according to the augmented and modified version<sup>57</sup> of an original thermodynamic database<sup>58</sup>. This is a result of (i) applying the Generator\_LINUX” module of LitMod2D\_2.0<sup>52,53</sup> which builds on the Perple\_X

algorithm<sup>54,55</sup> and (ii) correcting for anelastic attenuation effects using V2RhoT\_gibbs<sup>51</sup>; **b, c** illustration of the look-up table search performed using V2RhoT\_gibbs<sup>51</sup> for the  $v_s$ -tomography model CSEM Europe<sup>14</sup> (black points) within the ( $v_s$ , pressure)-parameter spaces for temperature (**b**) and density (**c**) that are consistent with the distribution in **a**.

fraction as derived from solidus and liquidus computations for dry peridotite<sup>63,64</sup>.

For the sub-continental lithospheric mantle of central Europe, relative abundances of major oxides of the NCFMAS system have been obtained from whole-rock chemical analyses of xenolith samples collected, for example, in the Southern Bohemian Massif<sup>65</sup> (Lower Austria) or the Eger Rift<sup>66</sup> (Southern Poland; Supplementary Table 1). In addition, modal compositions have been published for various subareas, such as the Eifel<sup>67</sup> or the Eger Rift<sup>68</sup>. Collectively, the datasets indicate regional differences in the degrees of mantle depletion and refertilization (Iherzolite to harzburgite compositions), which has motivated researchers to propose either horizontal<sup>69</sup> or vertical<sup>70</sup> compositional zonation for the lithospheric mantle of central Europe. The overall scarcity of observational data, however, precludes us from spatially differentiating differently composed mantle domains prior to performing the  $v_s$ -conversions. Hence, we have assumed the mantle to be compositionally homogeneous, which effectively corresponds to a purely thermal interpretation of seismic velocity. This raises the question of to what extent any compositional differences generally would affect the  $v_s$ -conversions. We have compared a set of different mantle compositions in terms of their relations between pressure, temperature,  $v_s$  and density (Supplementary Methods, Supplementary Figs. 2–5). Therefore, we have extended the range of analyzed chemical compositions to set the locally published ones<sup>65,66</sup> in relation to differently depleted standard compositions for both subcontinental<sup>71</sup> and mid-ocean ridge<sup>72</sup> mantle. Similar to what has been demonstrated before<sup>73</sup>, also our analysis shows that mantle compositions of very different degrees of depletion would result in essentially the same  $v_s$ -converted temperature (primarily varying by  $\pm 2^\circ$  C; Fig. Supplementary Fig. 5). Using a homogeneous mantle composition thus does not challenge the temperature configurations presented above. As it is comparable to the bulk-rock chemical compositions in the study area, we have chosen a more depleted type of subcontinental lithospheric mantle called Pr\_1<sup>71</sup>, which is a garnet-bearing harzburgite with a magnesium number of Mg#=90.6 and containing 0.15% Na<sub>2</sub>O, 1.9% CaO, 7.9 FeO, 42.4% MgO, 2.1% Al<sub>2</sub>O<sub>3</sub>, and 44.7% SiO<sub>2</sub>. Our analysis shows that assuming a lesser degree of depletion for the subcontinental lithospheric mantle

instead (by choosing a Iherzolitic composition) will result in differences of the  $v_s$ -converted density of around 20–25 kg·m<sup>-3</sup> over the analyzed ( $v_s$ , P)-range of the tomographic model (Supplementary Fig. 5). However since this density surplus of the Iherzolitic mantle with respect to a harzburgite is constant across the relevant parameter space, the spatial density patterns presented above would essentially remain the same (with homogeneously shifted absolute density values).

The input for our  $v_s$ -conversions is a regional excerpt of the second generation of the Collaborative Seismic Earth Model<sup>14</sup>, the latter being a collection of regional seismic tomographies compiled into a single global tomographic model. Submodels within the collaborative framework are based on full-waveform inversion, a seismic inverse method that efficiently exploits entire seismogram records by repeatedly solving the elastic wave equation<sup>74,75</sup>. This approach implies greater volumetric sensitivity to any subsurface heterogeneities compared to travel-time tomography. In the study area (11°W to 16°E, 45° to 60°N), CSEM Europe<sup>14</sup> combines information from previously published models<sup>76–78</sup> and the global CSEM inversion<sup>14</sup>. The model explains seismic wave propagation to a minimum period of 25 s.

CSEM Europe<sup>14</sup> contains information on the anisotropic components of shear-wave velocity (vertical  $v_{sv}$  and horizontal  $v_{sh}$ ) from which we derived the Voigt average ( $v_s$ ) as proposed by an earlier study<sup>79</sup>:

$$v_s = \sqrt{\frac{1}{3}(v_{sh}^2 + 2v_{sv}^2)} \quad (1)$$

Figure 9 shows the conversion procedure, starting from the pre-calculated  $v_s$ -distribution as a function of pressure and temperature for the chosen mantle composition (Fig. 8a). To illustrate the automatized picking of parameter values (temperature, density) from the corresponding look-up tables (implemented in V2RhoT\_gibbs<sup>51</sup>), each ( $v_s$ , depth)-couple contained in CSEM Europe<sup>14</sup> for the study area is plotted on the corresponding fields of temperature (Fig. 9b) and density (Fig. 9c).

Based on the  $v_s$ -derived thermal configuration, we have calculated the mantle effective viscosity ( $\eta$ ) according to its exponential dependence on

temperature and its power-law dependence on strain rate<sup>80</sup>:

$$\eta = \frac{2^{1-n}}{3^{1+n}} A_p^{-1} \varepsilon^{n-1} \exp\left(\frac{Q_p}{nRT}\right) \quad (2)$$

where  $A_p$  is the pre-exponential scaling factor for dislocation creep,  $n$  the power law exponent,  $Q_p$  the creep activation enthalpy,  $T$  the temperature and  $R$  is the universal gas constant ( $R = 8.314 \text{ J K}^{-1} \text{ mol}^{-1}$ ). Assuming a dry mantle composition (dry peridotite<sup>81</sup>), we have set  $A_p = 5.011e - 17 \text{ Pa}^{-n} \text{ s}^{-1}$ ,  $n = 3.5$  and  $Q_p = 5.35e + 03 \text{ J mol}^{-1}$ . Also note that we have fixed the reference strain rate to a constant value of  $\dot{\varepsilon} = 1e - 16 \text{ s}^{-1}$  for the calculations, which is lower than (but of the same order of magnitude as) the value of 5–10 nanostrain per year as assessed for the tectonically more active Alpine orogen<sup>2</sup>.

The earthquake catalog primarily used for this study has originally been compiled for a probabilistic seismic hazard assessment for the entire Euro-Mediterranean region (ESHM20 catalog<sup>3</sup>). It is collected from both historical and instrumental catalogs (years 1000–2014), includes >60,000 natural events, is harmonized in terms of magnitude scales, declustered, and checked for its magnitude of completeness (which is  $M_c \geq 4.5^3$ ). For our analysis of the seismicity distribution in western and Central Europe with respect to upper mantle heterogeneities we have extracted all ( $N = 1735$ ) seismic events of moment magnitudes  $M_w \geq 3.0$  located outside the Alpine and Fennoscandian regions of strongest present-day uplift<sup>2</sup> (white-covered area in the maps above). The advantage of using this cross-national, unified catalog for our study, of course, lies in its wide spatial coverage. Note that no matter if we resort to more complete national catalogs instead or change the magnitude range considered (Supplementary Methods; Supplementary Table 2; Supplementary Figs. 6–8), the primary trends in correlations between seismic activity and mantle heterogeneity remain the same. This is due to the fact that different catalogs or different minimum magnitude cut-offs capture the same first-order seismicity clustering within a few well-defined earthquakes zones, such as the N-S striking belt through mainland Britain, the South Armorican Seismic Zone, or the different segments of the ECRIS (Fig. 3b).

### Data availability

The input mantle tomography data (CSEM Europe<sup>14</sup>) for the region studied here is freely available for download via the following link: <https://zenodo.org/records/10600571><sup>82</sup>.

### Code availability

Tomographic shear-wave velocity (CSEM Europe<sup>14</sup>) has been converted to temperature and density with the open-source Python application V2RhoT\_gibbs<sup>51</sup> (<https://doi.org/10.5281/zenodo.6538257>), thereby opting for parameters as described in the above Methods section. Maps and profiles have been generated with GMT Version 6 (©Copyright 2019–2023, The GMT Developers<sup>83</sup>). For fairly presenting the data in maps and profiles, we have used Scientific Color Maps<sup>84</sup>. Figures have partly been finalized with the commercial packages CorelDraw Version 17 (©Corel Corporation 2014) and MS PowerPoint.

Received: 11 December 2023; Accepted: 24 April 2024;

Published online: 09 May 2024

### References

- Calais, E., Camelbeeck, T., Stein, S., Liu, M. & Craig, T. A new paradigm for large earthquakes in stable continental plate interiors. *Geophys. Res. Lett.* **43**, 637 (2016).
- Piña-Valdés, J. et al. 3D GNSS velocity field sheds light on the deformation mechanisms in Europe: effects of the vertical crustal motion on the distribution of seismicity. *J. Geophys. Res. Solid Earth* **127**, e2021JB023451 (2022).
- Danciu, L. et al. The 2020 update of the European Seismic Hazard Model-ESHM20: model overview. EFEHR Technical Report, **1** (2021).
- Heidbach, O. et al. The World Stress Map database release 2016: Crustal stress pattern across scales. *Tectonophysics* **744**, 484–498 (2018).
- Craig, T. J., Calais, E., Fleitout, L., Bollinger, L. & Scotti, O. Time-variable strain and stress rates induced by Holocene glacial isostatic adjustment in continental interiors. *Tectonophysics* **854**, 229815 (2023).
- Cloetingh, S. et al. Lithospheric memory, state of stress and rheology: neotectonic controls on Europe's intraplate continental topography. *Quat. Sci. Rev.* **24**, 241–304 (2005a).
- Brandes, C., Steffen, H., Steffen, R. & Wu, P. Intraplate seismicity in northern Central Europe is induced by the last glaciation. *Geology* **43**, 611–614 (2015).
- Mameri, L., Tommasi, A., Signorelli, J. & Hassani, R. Olivine-induced viscous anisotropy in fossil strike-slip mantle shear zones and associated strain localization in the crust. *Geophys. J. Int.* **224**, 608–625 (2021).
- Ottmüller, L. & Thomas, C. Highland Boundary Fault Zone: tectonic implications of the Aberfoyle earthquake sequence of 2003. *Tectonophysics* **430**, 83–95 (2007).
- Tesauero, M., Kaban, M. K., Cloetingh, S. A., Hardebol, N. J. & Beekman, F. 3D strength and gravity anomalies of the European lithosphere. *Earth Planet. Sci. Lett.* **263**, 56–73 (2007).
- Lebedev, S. et al. Seismicity of Ireland, and why it is so low. *Geophys. J. Int.* **235**, 431–447 (2023).
- Bezada, M. & Smale, J. Lateral variations in lithospheric mantle structure control the location of intracontinental seismicity in Australia. *Geophys. Res. Lett.* **46**, 12862–12869 (2019).
- Biryol, C. B., Wagner, L. S., Fischer, K. M. & Hawman, R. B. Relationship between observed upper mantle structures and recent tectonic activity across the southeastern United States. *J. Geophys. Res. Solid Earth* **121**, 3393–3414 (2016).
- Noe, S. et al. Collaborative seismic earth model: generation 2. *AGU Fall Meeting Abstracts* **2021**, S15E–S10298 (2021).
- Legendre, C., Meier, T., Lebedev, S., Friederich, W. & Viereck-Götte, L. A shear wave velocity model of the European upper mantle from automated inversion of seismic shear and surface waveforms. *Geophys. J. Int.* **191**, 282–304 (2012).
- Schaeffer, A. & Lebedev, S. Global shear speed structure of the upper mantle and transition zone. *Geophys. J. Int.* **194**, 417–449 (2013).
- Zhu, H., Bozdağ, E. & Tromp, J. Seismic structure of the European upper mantle based on adjoint tomography. *Geophys. J. Int.* **201**, 18–52 (2015).
- El-Sharkawy, A. et al. The slab puzzle of the Alpine-Mediterranean region: Insights from a new, high-resolution, shear wave velocity model of the upper mantle. *Geochem. Geophys. Geosyst.* **21**, e2020GC008993 (2020).
- Steinberger, B. Topography caused by mantle density variations: observation-based estimates and models derived from tomography and lithosphere thickness. *MNRAS* **205**, 604–621 (2016).
- Davies, D. R. et al. Earth's multi-scale topographic response to global mantle flow. *Nat. Geosci.* **12**, 845–850 (2019).
- Coblentz, D., Van Wijk, J., Richardson, R. M. & Sandiford, M. The upper mantle geoid: implications for continental structure and the intraplate stress field. *Geol. Soc. Am. Spec. Pap.* **514**, 197–214 (2015).
- Salajegheh, F. & Afonso, J. C. The upper mantle geoid for lithospheric structure and dynamics. *J. Geophys. Res. Solid Earth* **128**, e2023JB026397 (2023).
- Arrowsmith, S. J., Kendall, M., White, N., VanDecar, J. C. & Booth, D. C. Seismic imaging of a hot upwelling beneath the British Isles. *Geology* **33**, 345–348 (2005).
- Medhus, A. et al. Upper-mantle structure beneath the Southern Scandes Mountains and the Northern Tornquist Zone revealed by P-wave traveltimes tomography. *Geophys. J. Int.* **189**, 1315–1334 (2012).

25. Ritter, J. R., Jordan, M., Christensen, U. R. & Achauer, U. A mantle plume below the Eifel volcanic fields. *Germany. Earth Planet. Sci. Lett.* **186**, 7–14 (2001).
26. Granet, M., Wilson, M. & Achauer, U. Imaging a mantle plume beneath the French Massif Central. *Earth Planet. Sci. Lett.* **136**, 281–296 (1995).
27. Karousová, H., Plomerová, J. & Babuška, V. Upper-mantle structure beneath the southern Bohemian Massif and its surroundings imaged by high-resolution tomography. *Geophys. J. Int.* **194**, 1203–1215 (2013).
28. Achauer, U. & Masson, F. Seismic tomography of continental rifts revisited: from relative to absolute heterogeneities. *Tectonophysics* **358**, 17–37 (2002).
29. Evans, K. F., Zappone, A., Kraft, T., Deichmann, N. & Moia, F. A survey of the induced seismic responses to fluid injection in geothermal and CO<sub>2</sub> reservoirs in Europe. *Geothermics* **41**, 30–54 (2012).
30. Leclère, H. & Calais, É. A parametric analysis of fault reactivation in the New Madrid Seismic Zone: the role of pore fluid overpressure. *J. Geophys. Res. Solid Earth* **124**, 10630–10648 (2019).
31. Bräuer, K., Kämpf, H., Niedermann, S. & Wetzell, H.-U. Regional distribution pattern of carbon and helium isotopes from different volcanic fields in the French Massif Central: evidence for active mantle degassing and water transport. *Chem. Geol.* **469**, 4–18 (2017).
32. Fischer, T. et al. Intra-continental earthquake swarms in West-Bohemia and Vogtland: a review. *Tectonophysics* **611**, 1–27 (2014).
33. van Laaten, M., Wegler, U. & Eulenfeld, T. On the trail of fluids in the northernmost intracontinental earthquake swarm areas of the Leipzig-Regensburg fault zone, Germany. *J. Seismol.* **24**, 1–25 (2023).
34. Mazzotti, S. & Gueydan, F. Control of tectonic inheritance on continental intraplate strain rate and seismicity. *Tectonophysics* **746**, 602–610 (2018).
35. Chadwick, R., Pharaoh, T., Williamson, J. & Musson, R. Seismotectonics of the UK. Final report. BGS Technical Report Report No. WA/96/3C: Issue 1.0, (British Geological Survey, Keyworth, Nottingham, 1996).
36. Mazzotti, S., Jomard, H. & Masson, F. Processes and deformation rates generating seismicity in metropolitan France and conterminous Western Europe. *In: Bulletin de la Société Géologique de France* **191** (2020).
37. Hahn, T. et al. Seismotectonic regions in Germany and adjacent areas - concept and results. *in DGG 81. Jahrestagung 2021*. <https://doi.org/10.23689/ridgeo-3948> (2021).
38. Zhan, Y., Hou, G., Kusky, T. & Gregg, P. M. Stress development in heterogeneous lithosphere: Insights into earthquake processes in the New Madrid Seismic Zone. *Tectonophysics* **671**, 56–62 (2016).
39. Saxena, A., Choi, E., Powell, C. A. & Aslam, K. S. Seismicity in the central and southeastern United States due to upper mantle heterogeneities. *Geophys. J. Int.* **225**, 1624–1636 (2021).
40. Bai, Y., Williams, S. E., Müller, R. D., Liu, Z. & Hosseinpour, M. Mapping crustal thickness using marine gravity data: methods and uncertainties. *Geophysics* **79**, G1–G10 (2014).
41. Becker, T. W. et al. Western US intermountain seismicity caused by changes in upper mantle flow. *Nature* **524**, 458–461 (2015).
42. Sandiford, M., Lawrie, K. & Brodie, R. S. Hydrogeological implications of active tectonics in the Great Artesian Basin, Australia. *Hydrogeol. J.* **28**, 57–73 (2020).
43. Ghelichkhan, S., Bunge, H.-P. & Oeser, J. Global mantle flow retrodictions for the early Cenozoic using an adjoint method: evolving dynamic topographies, deep mantle structures, flow trajectories and sublithospheric stresses. *Geophys. J. Int.* **226**, 1432–1460 (2021).
44. Handy, M. & Brun, J.-P. Seismicity, structure and strength of the continental lithosphere. *Earth Planet. Sci. Lett.* **223**, 427–441 (2004).
45. Pollitz, F. F. Lithosphere and shallow asthenosphere rheology from observations of post-earthquake relaxation. *Phys. Earth Planet. Inter.* **293**, 106271 (2019).
46. Mazabraud, Y., Béthoux, N., Guilbert, J. & Bellier, O. Evidence for short-scale stress field variations within intraplate central-western France. *Geophys. J. Int.* **160**, 161–178 (2005a).
47. Précigout, J., Prigent, C., Palasse, L. & Pochon, A. Water pumping in mantle shear zones. *Nat. Commun.* **8**, 15736 (2017).
48. Kumar, A., Cacace, M., Scheck-Wenderoth, M., Götze, H. J. & Kaus, B. J. Present-day upper-mantle architecture of the alps: insights from data-driven dynamic modeling. *Geophys. Res. Lett.* **49**, e2022GL099476 (2022).
49. Petit, C., de Barros, L., Duclaux, G. & Mazabraud, Y. Why are there no earthquakes in the intracratonic Paris Basin? Insights from flexural models. *Geosciences* **9**, 502 (2019).
50. Anikiev, D., Cacace, M., Bott, J., Gomez Dacal, M. L. & Scheck-Wenderoth, M. Influence of lithosphere rheology on seismicity in an intracontinental rift: the case of the Rhine Graben. *Front. Earth Sci.* **8**, 592561 (2020).
51. Kumar, A. V2RhoT\_gibbs: a python tool to convert seismic velocities to temperature and density using gibbs-free energy minimization v. 0.1.0 *Zenodo*, <https://doi.org/10.5281/zenodo.6538257>. (2022).
52. Afonso, J. C., Fernandez, M., Ranalli, G., Griffin, W. & Connolly, J. Integrated geophysical-petrological modeling of the lithosphere and sublithospheric upper mantle: methodology and applications. *Geochem. Geophys. Geosyst.* **9**, Q05008 (2008).
53. Kumar, A. et al. LitMod2D\_2. 0: An improved integrated geophysical-petrological modeling tool for the physical interpretation of upper mantle anomalies. *Geochem. Geophys. Geosyst.* **21**, e2019GC008777 (2020).
54. Connolly, J. A. Computation of phase equilibria by linear programming: a tool for geodynamic modeling and its application to subduction zone decarbonation. *Earth Planet. Sci. Lett.* **236**, 524–541 (2005).
55. Connolly, J. The geodynamic equation of state: what and how. *Geochem. Geophys. Geosyst.* **10**, Q10014 (2009).
56. Palme, H. & O'Neill, H. S. C. Cosmochemical estimates of mantle composition. *Treat. Geochem.* **2**, 568 (2003).
57. Afonso, J. C. & Zlotnik, S. The subductability of the continental lithosphere: the before and after story. *In: Arc-Continent Collision Frontiers in Earth Sciences* (eds D. Brown & P. D. (Eds.) Ryan) 53–86 (Springer, 2011).
58. Holland, T. & Powell, R. An internally consistent thermodynamic data set for phases of petrological interest. *J. Metamorph. Geol.* **16**, 309–343 (1998).
59. Kennett, B. & Engdahl, E. Traveltimes for global earthquake location and phase identification. *Geophys. J. Int.* **105**, 429–465 (1991).
60. Jackson, I. & Faul, U. H. Grain-size-sensitive viscoelastic relaxation in olivine: Towards a robust laboratory-based model for seismological application. *Phys. Earth Planet. Inter.* **183**, 151–163 (2010).
61. Afonso, J. C. et al. 3-D multiobservable probabilistic inversion for the compositional and thermal structure of the lithosphere and upper mantle: III. Thermochemical tomography in the Western-Central US. *J. Geophys. Res. Solid Earth* **121**, 7337–7370 (2016).
62. Hammond, W. C. & Humphreys, E. D. Upper mantle seismic wave attenuation: effects of realistic partial melt distribution. *J. Geophys. Res. Solid Earth* **105**, 10987–10999 (2000).
63. Hirschmann, M. M. Mantle solidus: experimental constraints and the effects of peridotite composition. *Geochem. Geophys. Geosyst.* **1**, 2000GC000070 (2000).
64. Winter, J. Principles of igneous and metamorphic petrology. 2nd edn, 702 (Prentice Hall, 2010).
65. Becker, H. Geochemistry of garnet peridotite massifs from lower Austria and the composition of deep lithosphere beneath a Palaeozoic convergent plate margin. *Chem. Geol.* **134**, 49–65 (1996).
66. Puziewicz, J., Koepke, J., Grégoire, M., Ntaflos, T. & Matusiak-Matek, M. Lithospheric mantle modification during Cenozoic rifting in Central

- Europe: evidence from the Księginki nephelinite (SW Poland) xenolith suite. *J. Petrol.* **52**, 2107–2145 (2011).
67. Witt-Eickschen, G. & Kramm, U. Evidence for the multiple stage evolution of the subcontinental lithospheric mantle beneath the Eifel (Germany) from pyroxenite and composite pyroxenite/peridotite xenoliths. *Contrib. Miner. Petrol.* **131**, 258–272 (1998).
68. Kukuła, A. et al. Depleted subcontinental lithospheric mantle and its tholeiitic melt metasomatism beneath NE termination of the Eger Rift (Europe): the case study of the Steinberg (Upper Lusatia, SE Germany) xenoliths. *Miner. Petrol.* **109**, 761–787 (2015).
69. Puziewicz, J. et al. Three major types of subcontinental lithospheric mantle beneath the Variscan orogen in Europe. *Lithos* **362**, 105467 (2020).
70. Picazo, S. et al. Mapping the nature of mantle domains in Western and Central Europe based on clinopyroxene and spinel chemistry: Evidence for mantle modification during an extensional cycle. *Lithos* **266**, 233–263 (2016).
71. Griffin, W., O'Reilly, S. Y., Afonso, J. C. & Begg, G. The composition and evolution of lithospheric mantle: a re-evaluation and its tectonic implications. *J. Petrol.* **50**, 1185–1204 (2009).
72. Workman, R. K. & Hart, S. R. Major and trace element composition of the depleted MORB mantle (DMM). *Earth Planet. Sci. Lett.* **231**, 53–72 (2005).
73. Priestley, K. & McKenzie, D. The thermal structure of the lithosphere from shear wave velocities. *Earth Planet. Sci. Lett.* **244**, 285–301 (2006).
74. Tarantola, A. Inversion of seismic reflection data in the acoustic approximation. *Geophysics* **49**, 1259–1266 (1984).
75. Fichtner, A., Bunge, H.-P. & Igel, H. The adjoint method in seismology: I. Theory. *Phys. Earth Planet. Inter.* **157**, 86–104 (2006).
76. Fichtner, A. et al. Multiscale full waveform inversion. *Geophys. J. Int.* **194**, 534–556 (2013).
77. Rickers, F., Fichtner, A. & Trampert, J. The Iceland–Jan Mayen plume system and its impact on mantle dynamics in the North Atlantic region: evidence from full-waveform inversion. *Earth Planet. Sci. Lett.* **367**, 39–51 (2013).
78. Krischer, L., Fichtner, A., Boehm, C. & Igel, H. Automated large-scale full seismic waveform inversion for North America and the North Atlantic. *J. Geophys. Res. Solid Earth* **123**, 5902–5928 (2018).
79. Babuska, V. & Cara, M. Seismic anisotropy in the earth. Vol. 10 (Springer Science & Business Media, 1991).
80. Burov, E. B. Rheology and strength of the lithosphere. *Mar. Pet. Geol.* **28**, 1402–1443 (2011).
81. Hirth, G. & Kohlstedt, D. L. Water in the oceanic upper mantle: implications for rheology, melt extraction and the evolution of the lithosphere. *Earth Planet. Sci. Lett.* **144**, 93–108 (1996).
82. Noe, S. Dataset related to article: “Density and strength variations in the mantle lithosphere and the distribution of intraplate earthquakes”. *Zenodo*, <https://zenodo.org/records/10600571> (2024).
83. Wessel, P. et al. The generic mapping tools version 6. *Geochem. Geophys. Geosyst.* **20**, 5556–5564 (2019).
84. Crameri, F. Scientific colour maps. *Zenodo*, <https://doi.org/10.5281/zenodo.1243862> (2018).
85. Tesauro, M., Kaban, M. K. & Cloetingh, S. A. EuCRUST-07: a new reference model for the European crust. *Geophys. Res. Lett.* **35**, L05313 (2008).
86. Bluck, B., Gibbons, W. & Ingham, J. Terranes. *Geol. Soc. Lond. Mem.* **13**, 1–4 (1992).
87. Beucier, É. et al. Characteristics and possible origins of the seismicity in northwestern France. *C. R. Geosci.* **353**, 53–77 (2021).
88. Pharaoh, T. et al. Tectonic evolution. In: Petroleum geological atlas of the Southern Permian Basin area, 25–57 (EAGE, 2010).
89. Kley, J. & Voigt, T. Late Cretaceous intraplate thrusting in central Europe: Effect of Africa-Iberia-Europe convergence, not Alpine collision. *Geology* **36**, 839–842 (2008).
90. Dèzes, P., Schmid, S. & Ziegler, P. Evolution of the European Cenozoic Rift System: interaction of the Alpine and Pyrenean orogens with their foreland lithosphere. *Tectonophysics* **389**, 1–33 (2004).
91. Seton, M. et al. A global data set of present-day oceanic crustal age and seafloor spreading parameters. *Geochem. Geophys. Geosyst.* **21**, e2020GC009214 (2020).
92. Pharaoh, T. The Anglo-Brabant Massif: Persistent but enigmatic palaeo-relief at the heart of western Europe. *Proc. Geol. Assoc.* **129**, 278–328 (2018).

## Acknowledgements

Ajay Kumar acknowledges funding from the Deutsche Forschungsgemeinschaft (DFG) through the project “Deformation patterns in relation to the deep configuration of the lithosphere of the Alps and their forelands (DEFORM)” within the Special Priority Program (SPP) (SCHE 674/8-1) “Mountain Building Processes in Four Dimensions (4DMB)”. Funding for Sebastian Noe was provided by the European Union’s Horizon 2020 research and innovation program under the Marie Skłodowska-Curie grant agreement No. 955515 (SPIN ITN). The authors would like to thank Mike Sandiford and two anonymous reviewers for their critical and constructive suggestions, which contributed to an improved final version of the manuscript.

## Author contributions

Judith Bott and Magdalena Scheck-Wenderoth have developed the research idea. Judith Bott has written the first version of the manuscript and performed the parameter conversions together with Ajay Kumar. Mauro Cacace contributed with his expertise on earthquake mechanisms, and Jan Inge Faleide with his knowledge of the regional tectonic setting. Sebastian Noe has provided dedicated extracts of the used  $v_s$ -tomographic model. All authors contributed to the evaluation, interpretation, and discussion of the results and the revisions of the manuscript.

## Funding

Open Access funding enabled and organized by Projekt DEAL.

## Competing interests

The authors declare no competing interests.

## Additional information

**Supplementary information** The online version contains supplementary material available at <https://doi.org/10.1038/s43247-024-01417-4>.

**Correspondence** and requests for materials should be addressed to Judith Bott.

**Peer review information** *Communications Earth and Environment* thanks Mike Sandiford and the other, anonymous, reviewer(s) for their contribution to the peer review of this work. Primary Handling Editors: Kim Welford and Joe Aslin. A peer review file is available.

**Reprints and permissions information** is available at <http://www.nature.com/reprints>

**Publisher’s note** Springer Nature remains neutral with regard to jurisdictional claims in published maps and institutional affiliations.

**Open Access** This article is licensed under a Creative Commons Attribution 4.0 International License, which permits use, sharing, adaptation, distribution and reproduction in any medium or format, as long as you give appropriate credit to the original author(s) and the source, provide a link to the Creative Commons licence, and indicate if changes were made. The images or other third party material in this article are included in the article's Creative Commons licence, unless indicated otherwise in a credit line to the material. If material is not included in the article's Creative Commons licence and your intended use is not permitted by statutory regulation or exceeds the permitted use, you will need to obtain permission directly from the copyright holder. To view a copy of this licence, visit <http://creativecommons.org/licenses/by/4.0/>.

© The Author(s) 2024